Nano Research

ISSN 1998-0124 CN 11-5974/O4
https://doi.org/10.1007/s12274-020-2772-2

Research Article

Quantum anomalous Hall effect in two-dimensional Cu-dicyanobenzene coloring-triangle lattice

Yixuan Gao[1,2], Yu-Yang Zhang[1,2,3], Jia-Tao Sun[4], Lizhi Zhang[1,2] (✉), Shengbai Zhang[5], and Shixuan Du[1,2,3,6] (✉)

[1] *Institute of Physics, Chinese Academy of Sciences, Beijing 100190, China*
[2] *University of Chinese Academy of Sciences, Beijing 100049, China*
[3] *CAS Center for Excellence in Topological Quantum Computation, Beijing 100190, China*
[4] *School of Information and Electronics, MIIT Key Laboratory for Low-Dimensional Quantum Structure and Devices, Beijing Institute of Technology, Beijing 100081, China*
[5] *Rensselaer Polytechnic Institute, Troy, New York 12180, USA*
[6] *Songshan Lake Materials Laboratory, Dongguan 523808, China*

Received: 14 February 2020 / **Revised:** 13 March 2020 / **Accepted:** 22 March 2020

ABSTRACT

Magnetic two-dimensional (2D) topological insulators with spontaneous magnetization have been predicted to host quantum anomalous Hall effects (QAHEs). For organic topological insulators, the QAHE only exists in honeycomb or Kagome organometallic lattices based on theoretical calculations. Recently, coloring-triangle (CT) lattice has been found to be mathematically equivalent to a Kagome lattice, suggesting a potential 2D lattice to realize QAHE. Here, based on first-principles calculations, we predict an organometallic CT lattice, Cu-dicyanobenzene (DCB), to be a stable QAH insulator. It exhibits ferromagnetic (FM) properties as a result of the charge transfer from metal atoms to DCB molecules. Moreover, based on the Ising model, the Curie temperature of the FM ordering is calculated to be around 100 K. Both the Chern numbers and the chiral edge states of the semi-infinite Cu-DCB edge structure, which occur inside the spin-orbit coupling band gap, confirm its nontrivial topological properties. These make the Cu-DCB CT lattice an ideal candidate to enrich the family of QAH insulators.

KEYWORDS

quantum anomalous Hall effect, organic topological insulators, coloring-triangle lattice, Kagome lattice

1 Introduction

Two-dimensional (2D) topological insulators (TIs) have attracted considerable research interests due to the protection of their edge states inside bulk band gap by the time reversal symmetry (TRS) [1–7]. These robust edge states have the potential in applications such as spintronics and quantum computation with the advantage of low-power-consumption [8]. 2D TIs are also termed quantum spin Hall (QSH) insulators because of their quantized Hall conductivity induced by an external magnetic field [4]. When a TI has an intrinsic magnetic exchange interaction, a quantized Hall conductivity can be observed inside the topologically nontrivial insulating gap without the external magnetic field due to the broken of the TRS. This leads to a quantum anomalous Hall effect (QAHE) [9, 10]. The QAHE was first observed experimentally by Chang et al. in thin films of chromium-doped $(Bi, Sb)_2Te$ below 30 mK [11]. To date, despite various theoretical predictions and the new developments in synthetic methods, an experimental observation of a higher-temperature QAHE is still a daunting challenge [11, 12]. Thus, it is highly desirable to search for innovative topological materials with intrinsic magnetization and subsequently the QAHE.

So far, most materials predicted for realizing the QAHE are inorganic. Recently, however, several theoretical works suggested the possibility of 2D organometallic frameworks as organic topological insulators (OTIs) [13], which are known to have potential advantages such as low costs, easy of fabrication, and mechanical flexibility. To date, 2D OTIs can be divided into two groups: In the first one, metal atoms bond with two molecule ligands forming honeycomb lattices with a magnetic ground state [14–17]. They are the OTIs with QAHE; in the second one, metal atoms bond with three molecule ligands forming a Kagome lattice with a non-magnetic ground state [18–21]. In order to realize QAHE in OTIs with the Kagome lattice, substitution of the noble metal atoms (Cu, Pb, Bi) with magnetic metal atoms (Mn, Co) [22–24] is required, which turns the non-magnetic ground state into a magnetic ground state. Recently, Liu et al. proposed that a coloring-triangle (CT) lattice [25] can host the Kagome band and predicted that such a CT lattice can exist in an Au overlayer on Ca_2N substrate, although the overlayer here is non-magnetic. Clearly, time is ripe to uncover a class of intrinsically magnetic 2D CT lattices to host the QAHE.

In this paper, we report for the first time an organometallic CT lattice, i.e., the Cu-dicyanobenzene (DCB) lattice, as a stable QAHE insulator. We find that its ferromagnetic (FM) state, with local magnetic moments, comes from a charge transfer between the metal atoms and DCB molecules. The FM ordering is studied with the Ising model, which yields a Curie temperature for the Cu-DCB CT lattice at about 100 K. The calculated Chern numbers and the semi-infinite chiral edge states within the spin-orbit coupling (SOC) gap confirm its nontrivial topological

Address correspondence to Lizhi Zhang, lzhang94@utk.edu; Shixuan Du, sxdu@iphy.ac.cn

properties. Our findings suggest that Cu-DCB could be an ideal material for realizing QAHE.

2 Results and discussion

Figure 1 shows the structure of optimized freestanding 2D Cu-DCB CT lattice containing a hexagonal (honeycomb) lattice formed by Cu atoms (red dashed line), and a CT lattice formed by DCB molecules (blue shadows). In each unit cell (black rhombus in Fig. 1), there are two Cu atoms and three DCB molecules; the optimized lattice constant of the freestanding Cu-DCB CT lattice is a =17.63 Å. One DCB molecule contains one benzene ring and two CN groups (bottom left in Fig. 1). The DCB molecule can form strong coordination bonds with transition metal atoms due to its lone pair electrons of the CN group [26, 27]. The bond length and bond energy of Cu–N are about 1.87 Å and 1.08 eV, respectively. $E_{bond} = -(E_{tot} - 3 \times E_{mol} - 2 \times E_{Cu})/6$, where E_{tot} is the total energy of the lattice, E_{mol} is the energy of a free DCB molecule, and E_{Cu} is the energy of a free Cu atom). Molecular dynamics (MD) simulation at room temperature (RT) (Fig. S1 in the Electronic Supplementary Material (ESM)) demonstrates that Cu-DCB CT lattice is stable at RT.

We calculated the total energies of the Cu-DCB CT lattice in FM, antiferromagnetic (AFM) and nonmagnetic (NM) states. The results indicate that the FM state (Fig. 2(a)) is more stable than the AFM (Fig. 2(b)) and NM states by about 65 and 303 meV/unit cell, respectively. Although the energy differences normalized to atom are lower than the thermal energy at RT, the local magnetic moments in the DCB molecule are robust against structural distortion. The thermal stability of the FM ordering of these local magnetic moments can be evaluated using Monte Carlo simulations within the Ising model, which exhibits a Curie temperature of about 100 K, as illustrated in Fig. 2(c). Figures 2(a) and 2(b) show the spatial distributions of spin-polarized electron density in FM and AFM states, respectively. The spin-polarization in FM state mainly comes from the p_z orbitals of carbon and nitrogen atoms in the DCB molecules, resulting in a magnetic moment of 2.0 μ_B per unit cell. The spin-polarization in AFM state also comes from p_z orbitals of DCB molecules with a net spin of zero.

To better understand the intrinsic FM state of Cu-DCB CT lattice, we perform a molecular orbital analysis. From the electronic configuration of the Cu atom ($3d^{10}4s^1$), one can conclude that each Cu atom offers one extra electron to the DCB molecule. In accordance, the Bader charge analysis shows

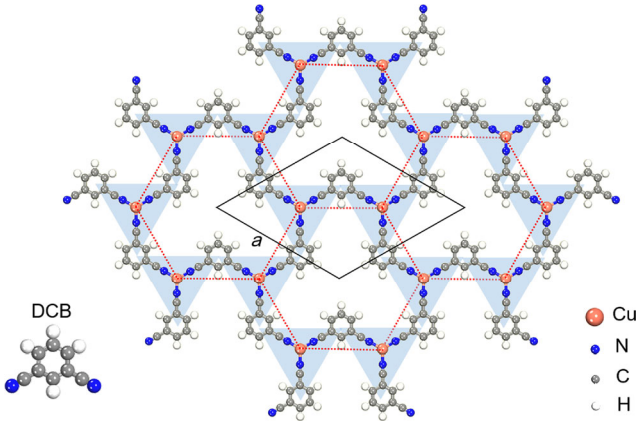

Figure 1 The atomic structure of Cu-DCB CT lattice. The bottom left inset shows the DCB molecular unit. The red dashed line and black rhombus outline the honeycomb lattice of Cu atoms and the unit cell, respectively. The blue shadows represent the CT lattice of the DCB molecules.

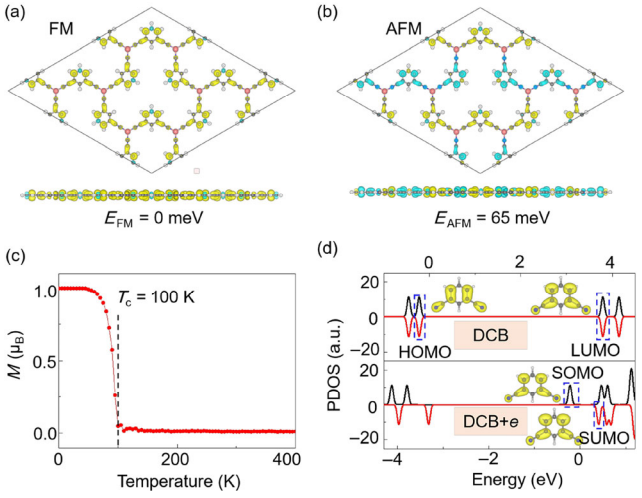

Figure 2 Magnetic properties of Cu-DCB CT lattice. The spatial distributions of spin-polarized electron density in (a) FM and (b) AFM states, where the iso-surface value is set to 0.002 e/Bohr^3. (c) Temperature dependence of magnetic moment calculated by using Ising model. (d) Molecular orbital analysis of intrinsic DCB molecule (upper panel) and the DCB molecule doped by one electron (lower panel).

that about 0.8 electrons are transferred from Cu atom to DCB molecule. Thus, we infer that the FM state is induced by an electron doping of the DCB molecules. To confirm, we calculate a single molecule with one extra electron, while maintaining the charge neutrality by a compensating homogenous background charge. As shown in Fig. 2(d), the doped DCB molecule indeed exhibits the FM. Moreover, the lowest unoccupied molecular orbital (LUMO) of the intrinsic DCB molecule splits into a singly occupied/a singly unoccupied molecular orbital (SOMO/SUMO, blue dashed rectangles in Fig. 2(d)), which is similar with previous studies [28, 29]. Physically, the two electrons of the two Cu atoms in a Cu-DCB unit cell occupy, according to the Pauli exclusion principle, the three SOMOs of the three DCB molecules with the same spin direction, which leads to a net magnetic moment of 2.0 μ_B.

The band structure of the FM state without SOC is shown in Fig. 3(a). We can clearly see the typical Kagome bands around the Fermi level, consisting of one flat band above two Dirac bands. These properties are consistent with the band structure of a CT lattice [25].

We noticed that the Cu-dicyanoanthracene (Cu-DCA) Kagome lattice has the same valence electrons as our Cu-DCB CT lattice. However, the Fermi level of Cu-DCA Kagome lattice is between two Dirac bands and its ground state is non-magnetic [19]. For Cu-DCB CT lattice, the spin-up (red line) and spin-down (black line) bands split, and only the spin-up bands are left around the Fermi level. The Fermi level is exactly between the flat band and top Dirac band. We have also investigated the influence from the on-site Coulomb interaction to the band structures (U_{eff} = 3 and 4 eV as commonly used for Cu atoms [30, 31]), and have found that the band structures (Fig. S2 in the ESM) are almost the same as that in Fig. 3(a). From the projected density of states (PDOS) shown in Fig. 3(b), the Kagome bands mainly come from the p_z orbitals of the carbon and nitrogen atoms in DCB molecules with little contribution from the Cu d orbitals.

When the spin-orbit coupling (SOC) is taken into account, a band gap (Δ_1 = 2.0 meV) opens between the flat band and the top Dirac band, and the Fermi level lies exactly inside the SOC gap, as shown in the inset of Fig. 3(c). The Dirac point around −0.2 eV also opens a gap of Δ_2 = 0.6 meV. The two band

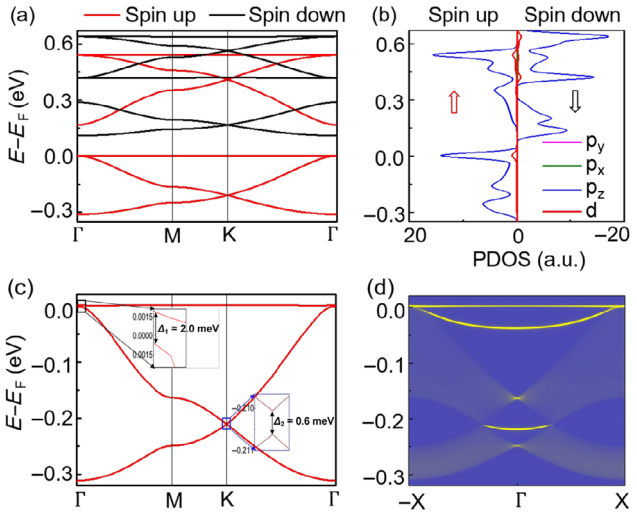

Figure 3 Electronic structures of the Cu-DCB CT lattice. (a) Band structure and (b) PDOS without SOC. (c) Band structure within SOC around two SOC gaps (Δ_1 = 2.0 meV and Δ_2 = 0.6 meV). (d) The semi-infinite chiral edge states within the SOC gaps (Δ_1 and Δ_2).

gaps can be further enlarged to Δ_1 = 2.5 meV and Δ_2 = 6.4 meV by placing the Cu-DCB CT on a monolayer h-BN (see Fig. S3 in the ESM). As an important signature of 2D TIs, the topological edge state of the Cu-DCB CT lattice is calculated by using the Wannier90 package [32], in which a tight-binding (TB) Hamiltonian in the basis of the maximally localized Wannier functions (MLWFs) is fitted to the first-principles band structure. Using these MLWFs, the edge Green's function of the semi-infinite CT lattice is constructed using the recursive method [33], and the local density of state (LDOS) of the edge structure is calculated. The LDOS for spin-up components of a semi-infinite Cu-DCB CT lattice is shown in Fig. 3(d). The nontrivial chiral topological edge states connecting the bottom of conduction band and top of valence band emerge in both SOC gaps (Δ_1 and Δ_2). A global band gap is opened when Cu is replaced by Au (see Fig. S4(d) in the ESM), due to its larger SOC than Cu. It separates the chiral edge states from the bulk states (see Fig. S4(e) in the ESM), which can be highly desirable in practical applications.

To further confirm the topological properties of the Cu-DCB bands, the Chern numbers C for spin polarized bands are calculated using the Kubo formula as follows

$$C = \frac{1}{2\pi}\int_{BZ} \mathrm{d}^2k\Omega(\boldsymbol{k})$$

$$\Omega(\boldsymbol{k}) = \sum_n f_n\Omega_n(\boldsymbol{k})$$

$$\Omega_n(\boldsymbol{k}) = -\sum_{n'\neq n} 2\mathrm{Im}\frac{\langle\psi_{n\boldsymbol{k}}|v_x|\psi_{n'\boldsymbol{k}}\rangle\langle\psi_{n'\boldsymbol{k}}|v_y|\psi_{n\boldsymbol{k}}\rangle}{(\varepsilon_{n'\boldsymbol{k}}-\varepsilon_{n\boldsymbol{k}})^2}$$

where n is the band index, $\psi_{n\boldsymbol{k}}$ is the eigenstate of eigenvalue $\varepsilon_{n\boldsymbol{k}}$ of band n, f_n is the Fermi distribution function, $v_{x/y}$ is the velocity operator. For the three Kagome bands, the flat band and the bottom Dirac band have a nonzero Chern number (±1), while the top Dirac band has a zero Chern number, as shown in Fig. 4(a). Thus, within the SOC gap of Δ_1 or Δ_2, the Chern number is 1. Apparently, the absolute value of the Chern number is consistent with the number of chiral edge state observed in each SOC gaps (Fig. 3(d)).

The existence of topological states of Cu-DCB CT lattice can be further manifested by calculated anomalous Hall conductivity

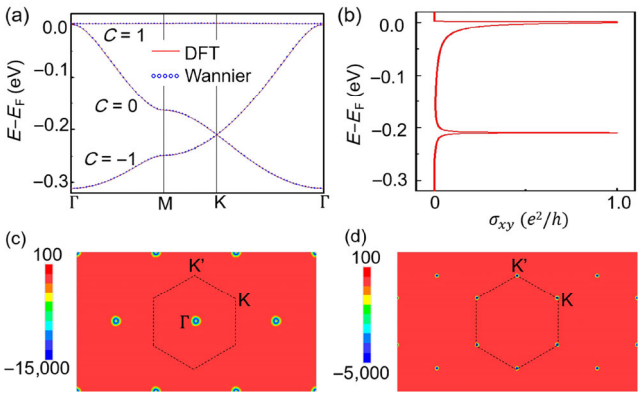

Figure 4 Topological properties of the Cu-DCB CT lattice. (a) The comparison between first-principles and Wannier band structures around two SOC gaps (Δ_1 and Δ_2). Chern numbers for each spin-polarized band are labeled. (b) Hall conductivity and distribution of the Berry curvatures in the Brillouin zone for flat (c) and bottom (d) Dirac band.

as a function of the nergy ($E - E_F$), as illustrated in Fig. 4(b). A quantized anomalous Hall conductivity plateau (e^2/h) is obtained within two SOC gaps (Δ_1 and Δ_2) from the Chern number as $\sigma_{xy} = C \times (e^2/h)$. Such a quantized Hall conductivity characterizes its non-trivial topological properties and confirms the existence of QAHE in the Cu-DCB CT lattice. We also give the distribution of Berry curvatures in Figs. 4(c) and 4(d). The Berry curvature of the flat band is mainly around the Γ point (Fig. 4(c)), while that of the bottom Dirac band is around the K point (Fig. 4(d)).

Moreover, the fractional quantum Hall effect could be possibly realized by further enlarging the energy gap and reducing the bandwidth of the flat band [18, 34, 35]. It is worth mentioning that the band gap is larger and band width of flat band is smaller (10.9 meV vs. 4.8 meV) when we substitute Cu atoms with Au atoms (see Fig. S4 in the ESM), suggesting that Au-DCB CT lattice is promising for fractional quantum Hall effect.

3 Conclusions

We predict QAHE in a new organometallic Cu-DCB CT lattice based on first-principles calculations. The Curie temperature estimated from Monte Carlo simulations within the Ising model can be as high as about 100 K. Moreover, the nontrivial properties of the Cu-DCB lattice are confirmed by the calculated nonzero Chern number, the quantized Hall conductivity, and the gapless chiral edge states. The stable Cu-DCB CT lattice is thus a promising candidate for achieving QAHE in experiment as well as for further device applications.

4 Methods

All density functional theory (DFT) calculations were carried out by using Vienna *ab initio* simulation package (VASP) with the projector augmented wave (PAW) method [36, 37]. A generalized gradient approximation (GGA) in the form of Perdew–Burke–Ernzerhof (PBE) was adopted for the exchange-correlation functional [38]. The wave functions were expanded using a planewave basis set with an energy cutoff of 600 eV. A Γ-centered 6 × 6 × 1 k-point mesh was used in the self-consistent calculations. In all the calculations, a 15 Å vacuum layer was used, and all atoms were fully relaxed until the residual forces on each atom were smaller than 0.01 eV/Å. Moreover, PBE+U calculations were also used to study the effects of on-site Coulomb interaction of transition metal. Here, we used the

method proposed by Dudarev et al. [39], where only the effective Coulomb interaction U_{eff} defined by the difference between the correlation energy and the exchange energy was meaningful. For Cu-DCB/h-BN system, the DFT-D3 method was used to correct the van der Waals interactions [40].

Acknowledgements

Work in China is supported by the National Natural Science Foundation of China (Nos. 51922011, 61888102, and 11974045), the National Key Research & Development Program of China (Nos. 2016YFA0202300, 2018YFA0305800, and 2019YFA0308500), the CAS Pioneer Hundred Talents Program, K. C. Wong Education Foundation, the Strategic Priority Research Program of Chinese Academy of Sciences (No. XDB30000000) and Beijing Institute of Technology Research Fund Program for Young Scholars. A portion of the research was performed in CAS Key Laboratory of Vacuum Physics. Computational resources were provided by the National Supercomputing Center in Tianjin. Work in the USA (S. B. Z.) was supported by U.S. DOE under Grant No. DE-SC0002623.

Electronic Supplementary Material: Supplementary material (molecular dynamics simulation of Cu-DCB CT lattice, band structures by using PBE+U method, relaxed configuration and band structure of Cu-DCB on h-BN surface, and electronic structures of Au-DCB CT lattice) is available in the online version of this article at https://doi.org/10.1007/s12274-020-2772-2.

References

[1] Hasan, M. Z.; Kane, C. L. *Colloquium*: Topological insulators. *Rev. Mod. Phys.* **2010**, *82*, 3045–3067.
[2] Qi, X. L.; Zhang, S. C. Topological insulators and superconductors. *Rev. Mod. Phys.* **2011**, *83*, 1057–1110.
[3] Kane, C. L.; Mele, E. J. Quantum spin Hall effect in graphene. *Phys. Rev. Lett.* **2005**, *95*, 226801.
[4] Bernevig, B. A.; Hughes, T. L.; Zhang, S. C. Quantum spin Hall effect and topological phase transition in HgTe quantum wells. *Science* **2006**, *314*, 1757–1761.
[5] Knez, I.; Du, R. R.; Sullivan, G. Evidence for helical edge modes in inverted InAs/GaSb quantum wells. *Phys. Rev. Lett.* **2011**, *107*, 136603.
[6] Zhou, M.; Ming, W. M.; Liu, Z.; Wang, Z. F.; Li, P.; Liu, F. Epitaxial growth of large-gap quantum spin Hall insulator on semiconductor surface. *Proc. Natl. Acad. Sci. USA* **2014**, *111*, 14378–14381.
[7] Gao, L.; Sun, J. T.; Sethi, G.; Zhang, Y. Y.; Du, S. X.; Liu, F. Orbital design of topological insulators from two-dimensional semiconductors. *Nanoscale* **2019**, *11*, 22743–22747.
[8] Liu, J. W.; Hsieh, T. H.; Wei, P.; Duan, W. H.; Moodera, J.; Fu, L. Spin-filtered edge states with an electrically tunable gap in a two-dimensional topological crystalline insulator. *Nat. Mater.* **2014**, *13*, 178–183.
[9] Haldane, F. D. M. Model for a quantum Hall effect without Landau levels: Condensed-matter realization of the "parity anomaly". *Phys. Rev. Lett.* **1988**, *61*, 2015–2018.
[10] Yu, R.; Zhang, W.; Zhang, H. J.; Zhang, S. C.; Dai, X.; Fang, Z. Quantized anomalous Hall effect in magnetic topological insulators. *Science* **2010**, *329*, 61–64.
[11] Chang, C. Z.; Zhang, J. S.; Feng, X.; Shen, J.; Zhang, Z. C.; Guo, M. H.; Li, K.; Ou, Y. B.; Wei, P.; Wang, L. L. et al. Experimental observation of the quantum anomalous Hall effect in a magnetic topological insulator. *Science* **2013**, *340*, 167–170.
[12] Checkelsky, J. G.; Ye, J. T.; Onose, Y.; Iwasa, Y.; Tokura, Y. Dirac-fermion-mediated ferromagnetism in a topological insulator. *Nat. Phys.* **2012**, *8*, 729–733.
[13] Wang, Z. F.; Liu, Z.; Liu, F. Organic topological insulators in organometallic lattices. *Nat. Commun.* **2013**, *4*, 1471.
[14] Yamada, M. G.; Soejima, T.; Tsuji, N.; Hirai, D.; Dincă, M.; Aoki, H. First-principles design of a half-filled flat band of the Kagome lattice in two-dimensional metal-organic frameworks. *Phys. Rev. B* **2016**, *94*, 081102.
[15] Sun, H.; Li, B.; Zhao, J. Half-metallicity in 2D organometallic honeycomb frameworks. *J. Phys. Condens. Matter* **2016**, *28*, 425301.
[16] Chen, Y.; Sun, Q. Magnetic two-dimensional organic topological insulator: Au-1,3,5-triethynylbenzene framework. *J. Chem. Phys.* **2017**, *147*, 104704.
[17] Zhang, X. M.; Zhao, M. W. Robust half-metallicity and topological aspects in two-dimensional Cu-TPyB. *Sci. Rep.* **2015**, *5*, 14098.
[18] Liu, Z.; Wang, Z. F.; Mei, J. W.; Wu, Y. S.; Liu, F. Flat Chern band in a two-dimensional organometallic framework. *Phys. Rev. Lett.* **2013**, *110*, 106804.
[19] Zhang, L. Z.; Wang, Z. F.; Huang, B.; Cui, B.; Wang, Z. M.; Du, S. X.; Gao, H. J.; Liu, F. Intrinsic two-dimensional organic topological insulators in metal-dicyanoanthracene lattices. *Nano Lett.* **2016**, *16*, 2072–2075.
[20] Sun, H.; Tan, S. J.; Feng, M.; Zhao, J.; Petek, H. Deconstruction of the electronic properties of a topological insulator with a two-dimensional noble metal-organic honeycomb-Kagome band structure. *J. Phys. Chem. C* **2018**, *122*, 18659–18668.
[21] Gao, Y. X.; Zhang, L. Z.; Zhang, Y. Y.; Du, S. X. Research progress of two-dimensional organic topological insulators. *Acta Phys. Sin.* **2018**, *67*, 238101.
[22] Wang, Y. P.; Ji, W. X.; Zhang, C. W.; Li, P.; Wang, P. J.; Kong, B.; Li, S. S.; Yan, S. S.; Liang, K. Discovery of intrinsic quantum anomalous Hall effect in organic Mn-DCA lattice. *Appl. Phys. Lett.* **2017**, *110*, 233107.
[23] Zhang, Y.; Wei, Z.; Zhang, M. G.; Gu, X.; Huang, L. Giant magnetic anisotropy of a two-dimensional metal-dicyanoanthracene framework. *Nanoscale* **2018**, *10*, 17335–17340.
[24] Wang, Z. F.; Liu, Z.; Liu, F. Quantum anomalous Hall effect in 2D organic topological insulators. *Phys. Rev. Lett.* **2013**, *110*, 196801.
[25] Zhang, S. H.; Kang, M.; Huang, H. Q.; Jiang, W.; Ni, X. J.; Kang, L.; Zhang, S. P.; Xu, H. X.; Liu, Z. et al. Kagome bands disguised in a coloring-triangle lattice. *Phys. Rev. B* **2019**, *99*, 100404.
[26] Zhang, Y. Y.; Du, S. X.; Gao, H. J. The construction and structure-property manipulation of "small-molecule machines". *Chin. Sci. Bull.* **2018**, *63*, 1255–1264.
[27] Cai, L. L.; Sun, Q.; Bao, M. L.; Ma, H. H.; Yuan, C. X.; Xu, W. Competition between hydrogen bonds and coordination bonds steered by the surface molecular coverage. *ACS Nano* **2017**, *11*, 3727–3732.
[28] Repp, J.; Meyer, G.; Paavilainen, S.; Olsson, F. E.; Persson, M. Imaging bond formation between a gold atom and pentacene on an insulating surface. *Science* **2006**, *312*, 1196–1199.
[29] Kumar, A.; Banerjee, K.; Dvorak, M.; Schulz, F.; Harju, A.; Rinke, P.; Liljeroth, P. Charge-transfer-driven nonplanar adsorption of F_4TCNQ molecules on epitaxial graphene. *ACS Nano* **2017**, *11*, 4960–4968.
[30] Lach, S.; Altenhof, A.; Tarafder, K.; Schmitt, F.; Ali, E.; Vogel, M.; Sauther, J.; Oppeneer, P. M.; Ziegler, C. Metal-organic hybrid interface states of a ferromagnet/organic semiconductor hybrid junction as basis for engineering spin injection in organic spintronics. *Adv. Funct. Mater.* **2012**, *22*, 989–997.
[31] Lee, K.; Howe, J. D.; Lin, L. C.; Smit, B.; Neaton, J. B. Small-molecule adsorption in open-site metal-organic frameworks: A systematic density functional theory study for rational design. *Chem. Mater.* **2015**, *27*, 668–678.
[32] Mostofi, A. A.; Yates, J. R.; Lee, Y. S.; Souza, I.; Vanderbilt, D.;

Marzari, N. Wannier90: A tool for obtaining maximally-localised Wannier functions. *Comput*. *Phys*. *Commun*. **2008**, *178*, 685–699.

[33] López Sancho, M. P.; López Sancho, J. M.; Rubio, J. Highly convergent schemes for the calculation of bulk and surface Green functions. *J*. *Phys*. *F Met*. *Phys*. **1985**, *15*, 851–858.

[34] Neupert, T.; Santos, L.; Chamon, C.; Mudry, C. Fractional quantum Hall states at zero magnetic field. *Phys*. *Rev*. *Lett*. **2011**, *106*, 236804.

[35] Tang, E.; Mei, J. W.; Wen, X. G. High-temperature fractional quantum Hall states. *Phys*. *Rev*. *Lett*. **2011**, *106*, 236802.

[36] Kresse, G.; Furthmüller, J. Efficiency of *ab-initio* total energy calculations for metals and semiconductors using a plane-wave basis set. *Comput*. *Mater*. *Sci*. **1996**, *6*, 15–50.

[37] Kresse, G.; Furthmüller, J. Efficient iterative schemes for *ab initio* total-energy calculations using a plane-wave basis set. *Phys*. *Rev*. *B* **1996**, *54*, 11169–11186.

[38] Perdew, J. P.; Burke, K.; Ernzerhof, M. Generalized gradient approximation made simple. *Phys*. *Rev*. *Lett*. **1996**, *77*, 3865–3868.

[39] Dudarev, S. L.; Botton, G. A.; Savrasov, S. Y.; Humphreys, C. J.; Sutton, A. P. Electron-energy-loss spectra and the structural stability of nickel oxide: An LSDA+U study. *Phys*. *Rev*. *B* **1998**, *57*, 1505–1509.

[40] Grimme, S.; Antony, J.; Ehrlich, S.; Krieg, H. A consistent and accurate *ab initio* parametrization of density functional dispersion correction (DFT-D) for the 94 elements H-Pu. *J*. *Chem*. *Phys*. **2010**, *132*, 154104.